RESEARCH PAPER

DEVELOPMENT OF LOW–COST ACTIVATED CARBON FROM CASHEW NUT SHELLS FOR METHYLENE BLUE DYE REMOVAL

B. Veeramani[1]. K. Raghu[2]*

[1,2] Department of Physics, Annamalai University, Chidambaram, Tamil Nadu, 608 002. INDIA

Corresponding author: raghuk.phy@gmail.com

ABSTRACT

This study investigates the removal of Methylene Blue (MB) dye from aqueous solutions using activated carbon derived from cashew nut shells (CNSAC). The adsorbent was synthesized through chemical activation using sodium hydroxide (NaOH) and characterized using XRD, SEM, FT-IR, BET, TG-DTA, and UV–Vis spectroscopy. The results showed that CNSAC possesses a high surface area and porous structure, which significant enhances its adsorption capacity. Batch adsorption experiments demonstrated efficient MB removal, achieving a maximum removal efficiency of 92% at an adsorbent dosage of 1.5 g/L. The adsorption data fitted well with the Langmuir isotherm model, suggesting monolayer adsorption. The adsorption kinetics were well described by the pseudo-second-order model, indicating that chemisorption may be the predominant rate-controlling mechanism. CNSAC also exhibited good stability and reusability, retaining 80% removal efficiency after five consecutive hydrothermal regeneration cycles. These findings demonstrate the potential of low-cost and environmentally friendly CNSAC as an effective adsorbent for dye removal from wastewater, contributing to sustainable water treatment practices.

How to cite this article: B. Veeramani1. K. Raghu2*. DEVELOPMENT OF LOW–COST ACTIVATED CARBON FROM CASHEW NUT SHELLS FOR METHYLENE BLUE DYE REMOVAL. Int J Drug Deliv Technol. 2026;16(87s):1653-1665 DOI: 10.25258/ijddt.16.87s.176.

INTRODUCTION

Methylene blue (MB) is a widelyused cationic dye in various applications, such as dyeingtextiles (silk, leather, plastics, paper, and cotton mordant with tannin), ink production, and office supplies like copying paper. However, its excessive use and improper disposal pose significant health risks, including tissue necrosis, high blood pressure, and quadriplegia, as MB can enter thehuman bodythroughthefoodchain [1,2].Due to these hazards, it is crucial to remove MB from wastewater effectively. The use of low-cost adsorbents has been globally recognized as an efficient, environmentally friendly solution for minimizing MB pollution [3-7]. Consequently, research has focused on identifying economically viable and effective adsorbents.

The environmental impact of syntheticdyes,likeMB, isconcerningdueto their complex aromatic molecular structures, which make them resistant to biodegradation. These dyes not only cause toxicological effects but also impair the aesthetic quality of water bodies by reducing light penetration, thereby disrupting aquatic ecosystems and threatening organisms with in the food chain[8].Furthermore,some synthetic dyes and their degradation byproducts are potentially carcinogenic, highlighting the need for their removal from wastewater [9]. Addressing these challenges necessitates interdisciplinary approaches, from developing innovative removal technologies to enforcing stringent regulations on dye-laden effluent discharges [10].Prioritizing the removal of such dyes is crucial for protecting water resources and maintaining environmental sustainability for future generations [11].

Traditional methods for color removal from wastewater, such as biological treatments and chemical precipitation, are effective only at high solute concentrations [12]. In contrast, adsorption has emerged as a superior method due to its cost-effectiveness, ease of operation, high efficiency, and biodegradability, making it suitable for treating concentrated dye solutions [13,14]. Activated carbon, especially when derived from natural materials like wood or coal, has been found to be highly effective in adsorbing dyes from wastewater [15]. However, the high cost of commercially available activated carbon has driven research toward finding more affordable alternatives [16]. Recent studies have focused on producing low-cost activated carbons from agricultural residues, such as plum kernels, cassava peels, bagasse, jute fibers, and other plant-based materials, offering a sustainable and economical approach to dye removal from wastewater [17,18].

This study explores the potential of activated carbon derived from cashew nut shells (CNSAC) as an effective adsorbentfor removing methylene blue from aqueous solutions. The research aims to assess the efficiency of CNSAC and analyze kinetic and equilibrium data to understand the adsorption mechanisms involved. By optimizing adsorption processes, this study contributes to advancing sustainable water purification technologies.

MATERIALSMETHODS

The cashew nut (CN) shells used in this study were collected from virudhachalamTaluk in

the Cuddalore district of Tamil Nadu, India. The shells were thoroughly washed with deionized water to remove any surface impurities and contaminants. To ensure complete drying, the washed shells were then oven-dried at 110°C for 24 hours. Once dried, the shells were ground and sieved to obtain particles smaller than 2 mm, which served as the precursor material for the synthesis of activated carbon.

For the synthesis, sodium hydroxide (NaOH) was employed as the activating agent to enhance the porosity and surface areaoftheactivatedcarbonderivedfromthe cashew nut shells. Methylene blue (MB), with the chemical formula $C_{16}H_{18}ClN_3S$ was selected as the target adsorbate to assess the adsorption properties of the synthesized activated carbon. All chemicals used in the study, including HCl and NaOH, were of analytical reagent grade with a purity of 99%, sourced from SD Merck Fine Chemicals, India. These chemicals were utilized as received, without any further purification. All glassware used in the experiments underwent thorough acid washing, and deionized water was consistently used for dilutions and sample preparations to maintain the accuracy and reliability of the experimental procedures.

Synthesis of activated carbons

The precursor materials, cashew nut shells, were impregnated in a 50% sodium hydroxide (NaOH) solution at a ratio of 2:1 (shell weight to NaOH). This impregnation was carried out under continuous stirring for 6 hours using a magnetic stirrer to ensure thorough mixing and uniform chemical activation. After impregnation, the samples were subjected to a drying and activation process, which involved heating at a controlled rate of 20°C per minute until reaching a fixed temperature of 500°C. This activation temperature was maintained for 2 hours to enhance the formation of pores and increase the surface area of the activated carbon.

Once the heating process was completed, the samples were allowed to cool naturally to room temperature. The cooled products were then thoroughly washed with 0.1 M hydrochloric acid (HCl) to remove any remaining sodium residues and mineral contaminants, followed by rinsing with distilled water until neutral pH was achieved. The washed samples were subsequently dried again at 110°C for 6 hours to ensure all moisture was removed. Finally, the activated carbon derived from cashew nut shells (CNSAC) was cooled to room temperature and stored in a desiccator to prevent any moisture absorption until further use in adsorption experiments.

Characterizations

The surface morphologies of the cashew nutshell and the activated cashew nut shell (CNSAC) were analyzed using various advanced characterization techniques. X-ray diffraction (XRD) was employed to determine the crystalline structure, while scanning electron microscopy coupled with energy dispersive X-ray analysis (SEM) (Supra 55, Zeiss, Germany) was used to observe the surface morphology and elemental composition. The thermal stability of the samples was evaluated by thermogravimetric analysis (TG-DTA) over a temperature range of 30 to 700 °C, using an SDT650 analyzer (Waters, Germany). Functional group analysis was performed using Fourier-transform infrared spectroscopy (FTIR) across a wavenumber range of 400–4000 cm^{-1} to identify the various chemical groups present on the surface of the materials.

Adsorbate

Methylene blue (MB), obtained from Merck, India, was used as the adsorbate without further purification. A stock solution of 1000 mg/L was prepared by dissolving the required amount of MB powder in double-distilled water. Working solutions of the required concentrations (50-250 mg/L) were prepared by diluting the stock solution with double-distilled water. The MB used was methylene blue hydrochloride trihydrate ($C_{16}H_{18}ClN_3S{\cdot}3H_2O$), with a molecular weight of 373.9 g/mol. Before adding the adsorbent, the pH of each solution was adjusted to the desired value using 0.1 M NaOH or 0.1 M HCl.

Analysis

The concentration of methylene blue (MB) in the supernatant solution, both before and after the adsorption process, was quantified using a double beam UV-visible spectrophotometer (Shimadzu, Japan) at a wavelength of 664 nm. The supernatant obtained from the CNSAC did not show any detectable absorbance at this wavelength, indicating the effective removal of MB. Additionally, the calibration curve employed in this study demonstrated high reproducibility and linearity across the concentration range used. The pH of the solution was accurately measured with a Hanna pH meter equipped with a combined glass electrode (Model HI 9025C, Singapore), ensuring precise control of experimental conditions.

Adsorption Experiment

Batch adsorption studies were performed at ambient temperature. For each adsorption experiment, a specific amount of CNSAC was added to a 250 mL Erlenmeyer flask containing 100 mL of the wastewater sample. The pH of the solution was adjusted to the desired level by adding either 0.1 M NaOH or HCl. The mixture of CNSAC and solution was then agitated for a predetermined duration using a wrist action shaker set at 120 rpm. The kinetics of adsorption were investigated by measuring the dye uptake at various time intervals. For accurate kinetic data, separate bottles containing 100 mL of wastewater and 0.15 g of CNSAC were utilized for each measurement point.

Isothermal adsorption studies were carried out with initial dye concentrations ranging from 50 to 250 mg/L, using 100 mL of the sample. These studies involved shaking the reaction mixture until equilibrium was reached. The concentration of the residual dye in the supernatant was determined by centrifuging the mixture and measuring the absorbance at the wavelength corresponding to the maximum absorbance of the dye. The dye concentration was then calculated using a pre-established calibration curve. It was observed that the λmax values of the wastewater samples varied by ±10 nm from the λmax values of the pure dyes at a constant pH. The amount of dye adsorbed onto the CNSAC, denoted as qe (mg/g), was computed using the following mass balance equation:

$$q_e = C_i - C_e V/w \text{---------- (1)}$$

Where Ci and Ce are the initial and equilibrium liquid-phase concentrations of dye, respectively (mg/L), V the volume of the solution (L), and W is the mass of the CNSAC used (g).

Regeneration studies

The reusability of CNSAC was evaluated over five consecutive adsorption-regeneration cycles. All regeneration studies were conducted in 150 mL Erlenmeyer flasks. In each cycle, adsorption was carried out using 1.5 g/L of CNSAC in 100 mL of MB solution (10 mg/L, pH 12 mg/L). After adsorption, the MB-loaded CNSAC was separated by filtration, washed with water and acetone, and dried. Regeneration was carried out hydrothermally by treating the spent adsorbent in water in an autoclave at 180 °C for 4 h, followed by reactivation at 500 °C under a nitrogen atmosphere. The regenerated CNSAC was then reused in the next adsorption experiment under the same conditions. The removal efficiency of each cycle was calculated to assess the effectiveness of the regeneration process.

RESULTS AND DISCUSSION

Thermal Analysis

Figure 1 represents the thermal gravimetric and differential thermal analysis (TG/DTA) curve for the raw cashew nut shell (CNS) precursor. The analysis reveals that the thermal decomposition of the raw CNS occurs in three distinct stages:

Stage 1: From room temperature up to 100°C, the TG curve shows an initial weight loss of approximately 4.75%. This loss is primarily due to the evaporation of moisture inherent in the CNS samples.

Stage 2: In the temperature range of 100°C to 225°C, the weight decreases by around 7.02%. This reduction is attributed to the release of organic volatiles and the decomposition of hemicellulose [19].

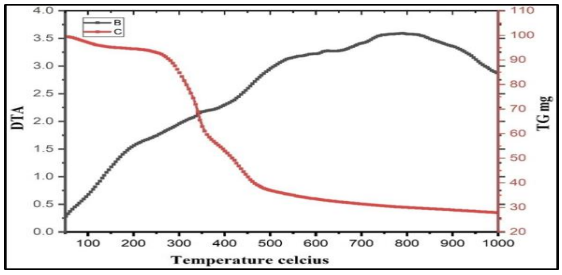


Figure .1 Thermal behaviour (TG/DTA curves) of CNSAC

Stage 3: Between 225°C and 350°C, the TG curve exhibits the most substantial weight loss, approximately 45.98%. This stage is associated with the decomposition of cellulose and lignin, which are the primary structural components of the CNS. This phase is marked by the maximum rate of weight loss, indicating the intensive breakdown of these components.

Beyond 350°C: The TG curve shows the formation of fixed carbon, which constitutes about 20.05% of the raw CNS [20]. Following 350°C, the weight loss becomes exponential, corresponding to the remaining 20.07% of fixed carbon. This behavior suggests a gradual conversion of residual organic matter into stable carbon.

For the preparation of activated carbon from CNS, it is advisable to use an activation temperature exceeding 350°C. This ensures thorough decomposition of volatile materials and the formation of a significant amount of fixed carbon, which is crucial for achieving high surface area and porosity in the activated carbon.

XRD analysis

Figure 2 illustrates the X-ray diffraction (XRD) patterns for activated carbon derived from cashew nut shells, synthesized under an impregnation ratio of 2:1 and a temperature of 500°C. The XRD analysis provides insights into the structural characteristics of the activated carbon.

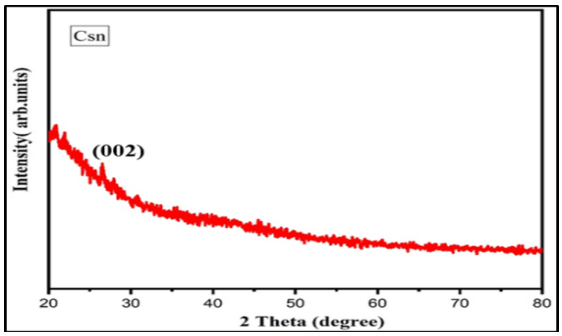


Figure .2 XRD pattern of CNSAC

The XRD patterns of the activated carbon primarily display broad, diffuse humps rather than sharp, well-defined peaks. This broadening is indicative of an amorphous carbon structure, which is a common feature in activated carbons. The absence of multiple distinct peaks suggests a lack of long-range order in the carbon lattice, typical for materials with high porosity and irregular structure. A notable sharp peak is observed at 2θ = 26°. This

peak is attributed to the (002) diffraction planes of microcrystalline graphite.

In the context of activated carbon, this peak signifies the presence of a small amount of graphitic structure embedded within the otherwise amorphous carbon matrix. The (002) planes correspond to the graphite layers' spacing, and their presence in the XRD pattern indicates that some degree of graphitization has occurred during the activation process.The peak at $2\theta = 26°$ aligns with the data from the JCPDS-751621 reference [21], which corresponds to the diffraction pattern of microcrystalline graphite. This reference confirms the identification of the sharp peak and supports the conclusion that while the activated carbon is predominantly amorphous, it contains regions of ordered graphite structures.

The presence of the (002) peak suggests that the activated carbon possesses some degree of graphitic ordering, which may contribute to its electronic properties and stability. However, the predominance of amorphous regions indicates that the material has a high surface area and significant porosity, essential for its adsorption capabilities. The balance between amorphous and graphitic structures can affect the overall performance of the activated carbon in applications such as adsorption, where high surface area and pore structure are crucial.

SEM Analysis

Figure 3 displays the scanning electron microscopy (SEM) micrographs of the cashew nut shell-derived activated carbon (CNSAC). The images reveal a distinct honeycomb-like porous morphology on the surface of the activated carbon.

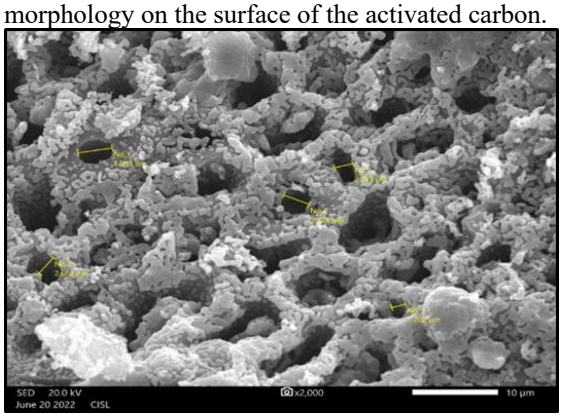


Figure 3. SEM image of CNSAC

This porous structure is indicative of an extensive internal surface area and aligns with the high iodine number previously reported for the activated carbon synthesized at the specified ratio.

The SEM micrographs illustrate a well-developed network of interconnected pores that form a honeycomb-like appearance. This intricate pore structure is characteristic of activated carbons with high surface areas and pore volumes. The visible pores are evidence of the successful activation process, which enhances the material's adsorptive properties.

The observed porous morphology correlates with the high iodine number obtained for the activated carbon. The iodine number is a standard measure of the micropore volume and surface area of activated carbon. A higher iodine number indicates a greater number of small micropores, which is consistent with the extensive pore structure shown in the SEM images. This relationship underscores the effectiveness of the activation process in creating a high surface area within the activated carbon.

The presence of a honeycomb-like porous surface and a large internal surface area is crucial for the functionality of activated carbon as an adsorbent. The extensive network of pores provides numerous sites for adsorption, enhancing the material's ability to capture and retain various adsorbates. The porous morphology ensures that the activated carbon can efficiently interact with and adsorb contaminants, making it suitable for applications in water treatment, air purification, and other adsorption-based processes [22].

FT-IR Analysis

Figure 4 presents the Fourier-transform infrared (FT-IR) spectrum of the activated carbon derived from cashew nut shells (CNSAC). The FT-IR analysis provides valuable insights into the chemical composition and surface functional groups of the CNSAC.

The prominent and broad band observed at 3428 cm^{-1} is attributed to the stretching vibrations of hydrogen-bonded hydroxyl groups. This peak suggests the presence of alcohols, phenols, and bound water molecules within the CNSAC structure. Additionally, this band may also indicate the presence of N-H bonds from primary amines [23], which are commonly found in activated carbons due to the incorporation of nitrogen-containing groups during the activation process.

The absorption bands located at 2974 cm^{-1} and 2854 cm^{-1} are associated with C-H stretching vibrations in aliphatic methyl groups. These bands highlight the presence of aliphatic hydrocarbons, contributing to the overall structural complexity of the activated carbon [24].

The sharp peaks at 1626 cm^{-1}, 1493 cm^{-1}, and 1453 cm^{-1} are indicative of C=C stretching vibrations in aromatic compounds [25]. These bands suggest the presence of aromatic ring structures within the activated carbon, which are characteristic of the carbonization process and contribute to the material's stability and adsorption properties.

The band observed at 1375 cm^{-1} is attributed to C-H in-plane bending vibrations in methylene groups. This peak further supports the presence of aliphatic components in the CNSAC structure.

The bands observed at 1242 cm^{-1}, 1105 cm^{-1}, and 1023 cm^{-1} are associated with C-O

stretching vibrations, which can be attributed to alcohols, phenols, ethers, or esters [26]. These bands indicate that the CNSAC contains various oxygen-containing functional groups, enhancing its surface chemistry and adsorption capacity.

The absorption band at 826 cm^{-1} corresponds to C-H out-of-plane bending vibrations in benzene derivatives. This peak signifies the presence of aromatic rings with substituted groups, contributing to the material's structural complexity.

The strong band at 614 cm^{-1} is associated with O-H bending vibrations [27]. This peak reflects the presence of hydroxyl groups and further corroborates the incorporation of oxygen-containing functionalities in the CNSAC.

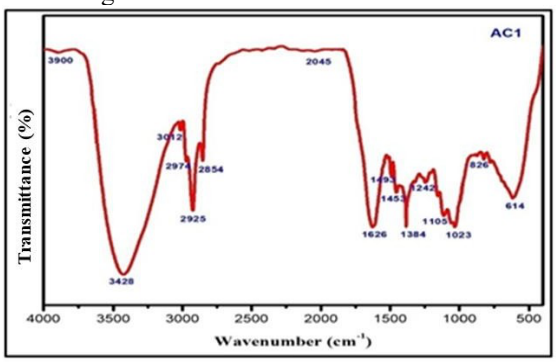


Figure 4. FT-IR spectra of CNSAC

BET Analysis of Cashew Nut Shell Activated Carbon: Surface Area, Pore Size Distribution, and Adsorption Properties

Activated carbon derived from cashew nut shells has been widely investigated for its adsorption capacity and structural characteristics [35, 36]. Brunauer-Emmett-Teller (BET) analysis is used to determine the specific surface area, pore volume, and pore size distribution of porous materials [38, 39].

The nitrogen adsorption-desorption isotherms of CNSAC (Fig. 5) resemble a Type IV isotherm, which is typical of mesoporous materials [38, 39]. Nitrogen uptake increases gradually at low relative pressures (p/p_0) and more steeply at higher pressures, indicating multilayer adsorption on the carbon surface. A hysteresis loop between the adsorption and desorption branches indicates the presence of mesopores, arising from capillary condensation within the pores.

The BET surface area of CNSAC was found to be 65.833 m^2/g, which provides sufficient accessible surface for the adsorption of dye molecules such as MB [35, 36].

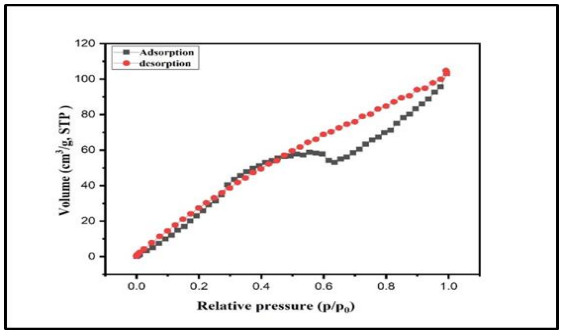


Fig 5: Nitrogen Adsorption-Desorption Isotherms of CNSAC

Pore Size Distribution

Pore size distribution is a vital parameter in understanding the performance of porous materials [35, 37]. Figure 6, which shows the pore size distribution for cashew nut shell activated carbon, reveals a sharp increase in pore volume for radii under 100 nm. This distribution suggests that the material has a high concentration of mesopores, contributing to its impressive adsorption capacity. The average pore diameter, calculated from BET analysis, is 0.078 nm, indicating the material's ability to facilitate efficient adsorption and transport of molecules within its pore network.

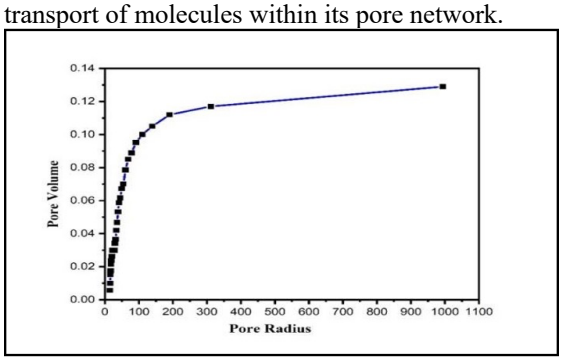


Fig 6: Pore radius curve of CNSAC

While the mesoporous structure dominates, the material also contains micropores, as evidenced by the low-pressure nitrogen adsorption behavior shown in Figure 7. The adsorption at low relative pressures ($p/p_0 < 0.3$) indicates the existence of micropores that provide an additional large surface area [37]. This combination of micropores and mesopores creates a hierarchical pore structure, beneficial for both rapid molecular transport (via mesopores) and high adsorption capacity (due to micropores).

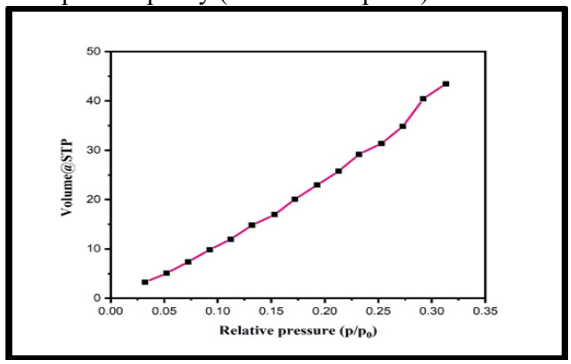


Fig 7: Volume @STP vs Relative Pressure

Total Pore Volume and Average Pore Diameter

The total pore volume of CNSAC was determined to be 0.129 cm^3/g, indicating a considerable pore network. The average pore diameter calculated from the pore size distribution curve is approximately 14.843 Å (1.4843 nm), which lies at the upper end of the micropore range. Together with the pore volume rising up to larger pore radii (Fig. 6), these values indicate a micro-mesoporous structure, in which the pore sizes are suitable for the adsorption of dye molecules such as MB [35, 36].

Adsorption Studies

Adsorption studies were conducted using the batch technique to determine the equilibrium data for the dye removal process. In each experiment, 0.15 g of the adsorbent was introduced into 100 mL of dye solution with a known initial concentration. Each experiment was replicated twice to ensure accuracy and reproducibility of the results. After allowing sufficient time for equilibrium to be reached, the final dye concentration (Ce) was measured. The percentage of dye removal was calculated using the formula:

Percentage Dye Removal= $(Ci - Ce)/Ci \times 100$ ----------(2)

whereCi and Ce represent the initial and equilibrium concentrations of the dye (in mg/L), respectively.

The amount of dye adsorbed per unit mass of the adsorbent (qe, in mg/g) was determined sbased on the mass balance principle, using the following equation

$q_e=(C_i - C_e)V/M$---------- (3)

where (V) is the volume of the dye solution (in L), and M is the mass of the adsorbent used (in g).

Batch adsorption experiments were conducted over a range of initial pH values from approximately 2 to 12. The initial pH of the solutions was adjusted by the addition of dilute hydrochloric acid (HCl) or sodium hydroxide (NaOH) solutions. pH values were accurately measured using an Elico brand pH meter to ensure precise control over the experimental conditions.

Additionally, the impact of temperature on the adsorption process was investigated by performing experiments at various temperatures, specifically 30°C, 40°C, 50°C, and 60°C. This analysis helps in understanding how temperature variations influence the adsorption efficiency and overall performance.

The equilibrium data obtained from the adsorption studies were analyzed using two common adsorption isotherm models: The Langmuir and Freundlich isotherms. The Langmuir isotherm assumes a monolayer adsorption onto a surface with a finite number of identical sites, while the Freundlich isotherm represents a multilayer adsorption on heterogeneous surfaces.

The characteristic parameters for each isotherm model were determined to provide insights into the adsorption mechanism and capacity of the adsorbent. This thorough analysis allows for a comprehensive understanding of the adsorption characteristics and the effectiveness of the adsorbent in dye removal applications.

Effect of contact time

Figure 8 illustrates the effect of contact time on the removal of Methylene Blue (MB) dye from 100 mL dye solutions with initial concentrations ranging from 50 to 250 mg/L using cashew nut shell activated carbon (CNSAC) as the adsorbent at room temperature. The dye removal increases rapidly during the initial 40 minutes, indicating the availability of numerous active adsorption sites on the CNSAC surface. These sites facilitate the rapid adsorption of dye molecules from the solution.

As the contact time increases, the rate of dye removal gradually decreases and approaches a nearly constant value at approximately 60 minutes. This behavior may be attributed to the gradual occupation of available adsorption sites by dye molecules, which reduces the number of vacant sites available for further adsorption.

The initial rapid adsorption followed by a slower uptake indicates a transition from rapid surface adsorption to a slower adsorption stage that may involve diffusion of dye molecules into the pores of the activated carbon. The nearly constant removal observed at longer contact times suggests that the adsorption process approaches equilibrium under the experimental conditions.

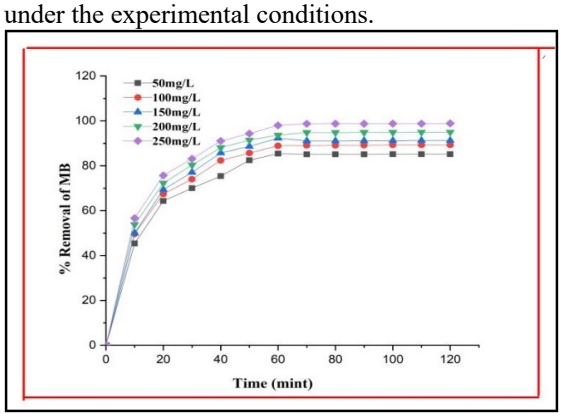


Figure 8: Effect of contact time on the adsorption of dye MB

Effect of solution pH

The influence of solution pH on the adsorption of' methylene blue (MB) was investigated by treating 100 mL of a 10 mg/L MB solution with 0.15 g of cashew nut shell activated carbon (CNSAC; dose 1.5 g/L), while varying the pH from 2 to 12. The results, depicted in Figure 9, show a marked variation in dye removal efficiency across the tested pH range. As illustrated, the percentage of MB removed from the solution increased significantly from 52.78% at pH 2 to 98.07% at pH 12. The highest removal efficiency was observed at pH 12, indicating that this is the optimum condition

for MB adsorption. Therefore, pH 12 was used for all subsequent adsorption experiments.

The lower adsorption efficiency at acidic pH (pH 2) can be attributed to the positively charged CNSAC surface at low pH, which electrostatically repels the cationic MB molecules. In addition, the excess hydrogen ions (H^+) in acidic solutions compete with the cationic dye molecules for the adsorption sites on the CNSAC surface, thereby reducing the adsorption capacity.

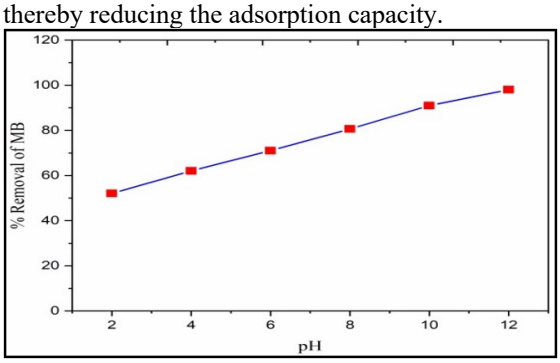


Figure 9:Effect of pH on %removal of MB

In contrast, at alkaline pH, particularly at pH 12, the surface functional groups of CNSAC deprotonate and the surface becomes negatively charged, which enhances the electrostatic attraction toward the cationic MB molecules. The reduced concentration of competing H^+ ions further facilitates the interaction between MB molecules and the active sites on CNSAC, leading to significantly higher dye removal efficiency.

This pH-dependent adsorption behavior underscores the importance of optimizing the pH to maximize the effectiveness of CNSAC as an adsorbent for dye removal [28].

Effect of adsorbent dosage

The effect of adsorbent dosage on the removal efficiency of methylene blue (MB) was studied by varying the dosage of cashew nut shell activated carbon (CNSAC) from 0.05 to 0.30 g per 100 mL of solution (0.5-3.0 g/L). These experiments were conducted with an initial MB concentration of 10 mg/L in 100 mL of solution at pH 12 and room temperature. The results are presented in Figure 10.

As shown, the percentage removal of MB increased markedly with the dosage of CNSAC up to 0.15 g/100 mL (1.5 g/L), from 67.8% at 0.05 g/100 mL to 98.07% at 0.15 g/100 mL. The most pronounced increase occurred between 0.05 and 0.15 g/100 mL. Beyond this point, further increases in dosage did not result in substantial gains in removal efficiency, indicating diminishing returns.

The increase in removal efficiency with dosage can be attributed to the greater surface area and number of available adsorption sites on CNSAC. At lower dosages, the limited number of active sites results in lower removal. As the dosage increases, more adsorption sites become available, which enhances the capture of MB molecules from the solution.

However, beyond the optimum dosage of 0.15 g/100 mL (1.5 g/L), additional adsorbent did not significantly enhance removal. This plateau indicates that most of the MB in solution had already been removed, so the additional adsorption sites contribute little further improvement. These findings underline the importance of optimizing the adsorbent dosage to achieve maximum dye removal while avoiding unnecessary use of adsorbent [28].

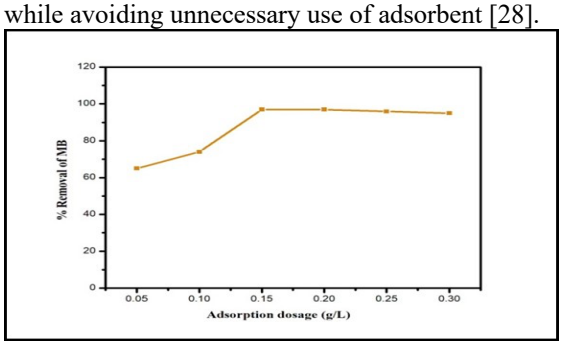


Figure 10. Effect of adsorbent dosage on the % removal of MB

Effect of initial dye concentration

Experiments were performed to evaluate the effect of initial dye concentration on the removal efficiency of Methyl Blue (MB) using an optimal adsorbent dose of 0.15 g in 100 mL dye solutions with varying concentrations of 50, 100, 150, 200, and 250 mg/L. The results, illustrated in Figure 11, show a clear trend in the percentage of MB removal as a function of initial dye concentration.

Effect of initial dye concentration

The effect of initial dye concentration on the removal efficiency of methylene blue (MB) was evaluated using the optimum adsorbent dose of 0.15 g in 100 mL of dye solution (1.5 g/L) at pH 12 and room temperature, with initial concentrations of 10, 20, 30, 40, and 50 mg/L. The results are illustrated in Figure 11.

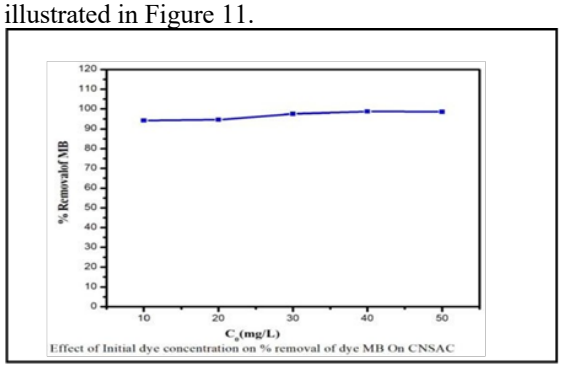


Figure 11. Effect of initial dye concentration on % removal of dye

As shown, the percentage removal of MB remained nearly constant at approximately 91-93% over the studied concentration range. This indicates that, at this dosage, CNSAC provides enough active sites to accommodate the dye molecules present in solution up to 50 mg/L, so the removal efficiency is not significantly affected by the increase in initial concentration. The slight

decrease at the highest concentration suggests that the adsorption sites are beginning to approach saturation. A higher initial concentration also increases the driving force for mass transfer of dye molecules from the solution to the CNSAC surface.

These results highlight the importance of considering both the adsorbent dosage and the initial dye concentration when designing efficient dye removal processes [29].

Adsorption Isotherms

Adsorption isotherms were determined from a series of batch adsorption experiments carried out at room temperature, employing an optimal adsorbent dosage of 1.5 g/L and an optimum pH of 12 for methylene blue (MB) dye. The contact time was set at 90 min to ensure adequate interaction between the adsorbent and the dye molecules. The initial concentration of MB in the aqueous solutions was varied systematically between 50 and 250 mg/L to investigate the adsorption capacity under different conditions.

During the adsorption process, samples were withdrawn from the reaction mixture at predefined time intervals and centrifuged to separate the adsorbent particles from the solution. The concentration of MB in the supernatant was then measured by UV-visible spectrophotometry at a wavelength of 664 nm, as shown in Fig. 12. From these measurements, the amount of dye adsorbed at different time intervals (q_t) and at equilibrium (q_e) was calculated.

The concentrations were determined using a previously established calibration curve correlating absorbance with dye concentration. These experimental data were then analyzed by fitting them to various adsorption isotherm models, such as the Langmuir and Freundlich isotherms, to understand the nature and capacity of the adsorption process. In addition, the adsorption kinetics were examined by applying different kinetic models, including the pseudo-first-order and pseudo-second-order models, to determine the mechanism controlling the adsorption rate and to elucidate the possible interaction between the dye molecules and the adsorbent surface.

The results demonstrated a clear trend in the adsorption behavior, confirming the efficacy of the adsorbent under the selected experimental conditions. As shown in Fig. 12, the absorbance of the supernatant decreased with time and eventually became constant, indicating that MB adsorption progressed and reached an equilibrium state. The fitting of the adsorption data to the isotherm and kinetic models provided further insights into the adsorption mechanism, which are crucial for optimizing the process for practical applications.

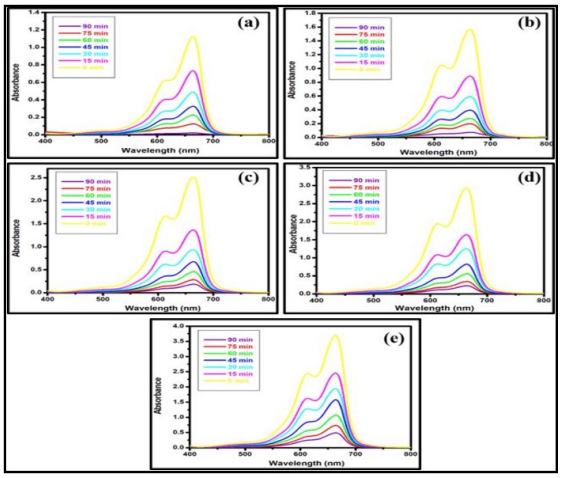


Figure 12. Absorption spectra of supernatant solution extracted from (a) 5% (b) 10 % (c) 15 % (d) 20% (e) 25 % MB solution at different intervals

Langmuir isotherm

The Langmuir isotherm model is based on the assumption that adsorption occurs as a monolayer on a surface containing a finite number of uniform adsorption sites. In this context, the adsorbate molecules adhere to the surface without any migration or movement across the surface plane once they are adsorbed.

The model further assumes that all adsorption sites are identical and possess the same energy, and that each site can accommodate only one adsorbate molecule, with no interactions occurring between adjacent adsorbed molecules. This model is particularly relevant for describing adsorption processes where the adsorbent surface is homogeneous, and the adsorption occurs in a single layer. The Langmuir isotherm is widely used to model adsorption in both liquid-solid and gas-solid systems, making it a versatile framework for understanding a wide range of adsorption phenomena.

$$q_e = q_m K_L C_e / (1 + K_L C_e) \text{----------(4)}$$

Where,$C_e$is the equilibrium concentration of the adsorbate in the solution (mg/L), q_e is the amount of adsorbate adsorbed per unit mass of the adsorbent at equilibrium (mg/g), $q_m$represents the maximum adsorption capacity, indicating the maximum amount of adsorbatethat can form a complete monolayer on the adsorbent surface (mg/g), and K is the Langmuir constant, which is related to the affinity or binding strength of the adsorbate to the adsorption sites (L/mg).

By fitting experimental data to the Langmuir isotherm model, the maximum adsorption capacity and the affinity of the adsorption sites for the adsorbate can be evaluated. The model is particularly effective in predicting the performance of adsorbents under controlled conditions where monolayer coverage is expected,

and it provides valuable insights into the nature and efficiency of the adsorption process.

Adsorption Kinetics

To elucidate the mechanisms governing the adsorption process, including mass transfer and chemical reactions, the experimental data were analyzed using various kinetic models, such as the pseudo-first-order, pseudo-second-order, and intraparticle diffusion models. Lagergren [32] first introduced the pseudo-first-order kinetic model for adsorption in solid-liquid systems, which is mathematically expressed as:

$dq_t/dt = k_1 (q_e - q_t)$ **----------(5)**

whereqt is the adsorption capacity at time t (mg/g), qe is the adsorption capacity at equilibrium (mg/g), and k_1 (min^{-1}) is the rate constant of the pseudo-first-order adsorption.

After integration by applying the initial conditions qt =0 at t=0 and $q_t = q_t$ at t=t, Eq.(2) becomes:

$\log(q_e - q_t) = \log q_e - (k_1 / 2.303)\, t$ (6) ----------(6)

Eq.(4) can be rearranged to obtain a linear form

$\text{Log}\ (q_e - q_t) = \log(q_e) - k_1/2.303\ (t)$----------(7)

In this study, the pseudo-first-order kinetic model was applied to analyze the adsorption of methylene blue (MB), where qtrepresents the adsorption capacity at time t (mg/g), and k_1(min^{-1}) is the rate constant. The rate constant $k_1$and the correlation coefficients for different dye concentrations were calculated from the linear plots of log ($q_e - q_t$) versus t(Fig. 13) and are presented in Table 1.

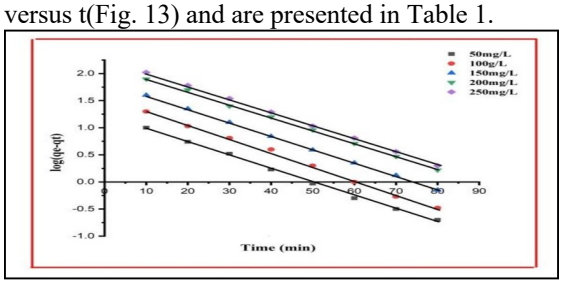


Figure 13. Pseudo – first order reaction for MB adsorbed onto CNSAC at different concentrations

The correlation coefficients for the pseudo-first-order model were found to be low, indicating that the model poorly fits the experimental data. Additionally, a significant discrepancy was observed between the experimental and calculated equilibrium adsorption capacities (q_e), further confirming that the pseudo-first-order model is inadequate for describing the adsorption process.

To provide a more accurate representation of the kinetics, the experimental data were analyzed using Ho's pseudo-second-order kinetic model, which assumes that the adsorption process follows a second-order chemisorption mechanism [34]. The model is expressed as:

$dq_t/dt = k_2 (q_e - q_t)^2$ ---------- (8)

Where, k is the rate constant of the pseudo-second-order adsorption (g mg−1min−1). Upon integrating this equation with the appropriate boundary conditions, the following linear form is obtained:

$(1/q_e - q_t) = 1/q_e + kt$----------8)

Eq.(7) can be rearranged to obtain a linear form:

$t/qt = 1/h + 1/q_e(t)$ ----------(9)

Where $h=k_2q$(mg $mg^{-1}min^{-1}$) represents the initial adsorption rate as t→0. If the adsorption process follows pseudo-second-order kinetics, a plot of t/q_t against t (Fig. 14) should yield a straight line.

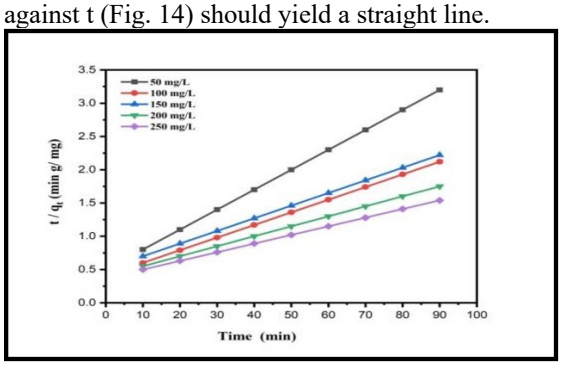


Figure 14. Pseudo – second order reaction for MB adsorbed onto CNSAC at different concentrations

From this plot, the parameters k, and h can be determined from the slope and intercept. The results showed that, for all initial dye concentrations studied, the plots produced straight lines with high correlation coefficients (>0.996).

Furthermore, the calculated values closely matched the experimental data, indicating that the pseudo-second order kinetic model accurately describes the adsorption process. These findings suggest that the rate-limiting step for MB adsorption onto CNSAC is likely chemisorption.

As shown in Table 1, the rate constant k decreases with increasing initial dye concentration for CNSAC. This trend can be attributed to reduced competition for adsorption sites at lower concentrations. In contrast, at higher concentrations, the competition for active surface sites intensifies, resulting in lower sorption rates.

To further understand the mechanisms and rate-controlling steps influencing the adsorption kinetics, the experimental data were also analyzed using Weber's intraparticle diffusion model [33]. This model helps clarify the diffusion mechanism and is expressed as:

$q_t = k_p t^{1/2} + C$---------- (10)

where C is the intercept, and k_p is the intraparticle diffusion rate constant (mg/g $min^{1/2}$). The constant $k_p$can be determined from the slope of the linear plot of qtversus $t^{1/2}$ [34], as shown in Fig. 15.

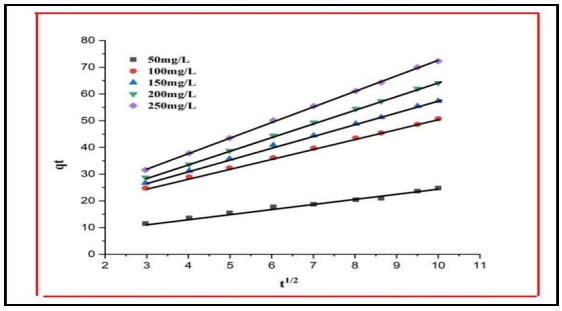


Figure 15.Intraparticle diffusion (MB concentrations=50-250 mg/L, adsorbent dose=1.5 g/L, volume of sample=100 mL and equilibrium time=90 min).

The intercept of the plot indicates the boundary layer effect, with a larger intercept suggesting a greater contribution of surface sorption to the rate-controlling step. The calculated values of the intraparticle diffusion coefficient, $k_p$are provided in Table 1. If the regression of qtversus $t^{1/2}$is linear and passes through the origin, it implies that intraparticle diffusion is the sole rate limiting step. However, the linear plots for each concentration did not pass through the origin, indicating that intraparticle diffusion is not the only rate-controlling step.

Table 1. Comparison between the adsorption rate constants, qe, estimated and correlation coefficients associated with pseudo-first-order and to the pseudo-second order rate equations and intraparticle diffusion

InitialMBconcent.(mg/L)	Pseudo–first ordermodal			Pseudo–secondordermodal					Intraparticled iffusion modal		
	K_1(min^{-1})	qe (mg/g)	R^2	K (gmg^{-1}min×10^{-3}	qecal (mg/g)	h (mgg^{-1}min^{-1})	qeexp(mg/g)	R^2	K p (mg/g.min1/2)	C	R^2
50	0.054	18.421	0.981	3.842	28.012	2.921	25.341	0.998	1.624	10.72	0.901
100	0.049	31.723	0.984	2.087	50.632	5.798	46.452	0.998	3.237	18.56	0.905
150	0.002	43.568	0.987	1.502	59.435	4.666	56.691	0.997	3.895	19.04	0.941
200	0.043	54.652	0.984	1.124	65.712	4.478	63.476	0.999	5.123	18.23	0.932
250	0.046	65.768	0.982	0.813	77.953	4.311	74.631	0.997	6.557	14.65	0.912

Stability and recyclability of the photo catalyst

The stability and reusability of photocatalysts are critical factors for their practical application, particularly in wastewater treatment processes. To evaluate the reusability of CNSAC, MB photodegradation experiments were conducted over five successive cycles. After each cycle, the spent CNSAC was recovered by filtration, thoroughly washed to remove residual contaminants, and subjected to hydrothermal regeneration before being reused in the subsequent photodegradation cycle. As illustrated in Fig. 16, the photodegradation efficiency of CNSAC showed a gradual decline over the five cycles, decreasing from 98% in the first cycle to 63% in the fifth cycle. This decrease may be attributed to the gradual loss of photocatalyst during recovery and the possible blockage or alteration of active sites after repeated hydrothermal regeneration. Nevertheless, CNSAC retained considerable photocatalytic activity after five regeneration cycles, demonstrating its potential for repeated use in MB photodegradation and wastewater treatment applications [34].

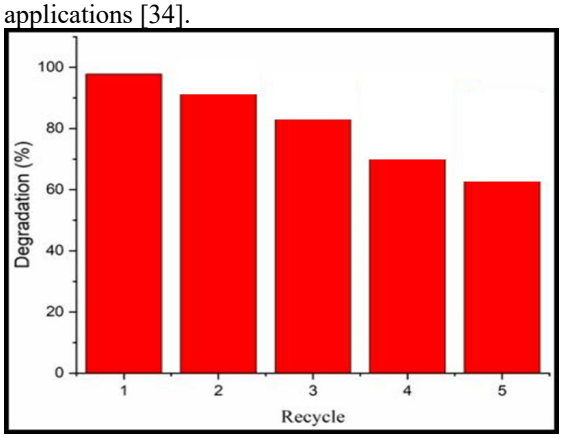


Fig.16. stability and reusability of the CNASC for photodegradation of MB

Hydrothermal Regeneration of Cashew Nut Shell Activated Carbon (CNS-AC)

Hydrothermal regeneration is a widely employed technique for restoring the adsorption capacity of spent activated carbon (AC) by desorbing adsorbed contaminants under high-temperature and high-pressure aqueous conditions. The regeneration process enhances the structural integrity of AC while preserving its surface properties for subsequent adsorption cycles. In this study, cashew nut shell-derived activated carbon (CNS-AC) underwent five cycles of hydrothermal regeneration, and the changes in its physicochemical properties were analyzed using adsorption isotherms, structural characterization, and surface functional group studies.

Hydrothermal Regeneration Procedure

The spent CNS-AC was washed with demonized water and dried at 105 °C for 12 h. The dried sample was placed in a Teflon-lined stainless steel autoclave containing demonized water and heated at 180 °C for 4 h to desorbs the adsorbed dye. After cooling naturally to room temperature, the carbon was filtered, washed with deionized water, and dried at 110 °C for 12 h. It was then reactivated in a tubular furnace at 500 °C under a nitrogen atmosphere to restore its porosity. This cycle was repeated for five regeneration cycles.

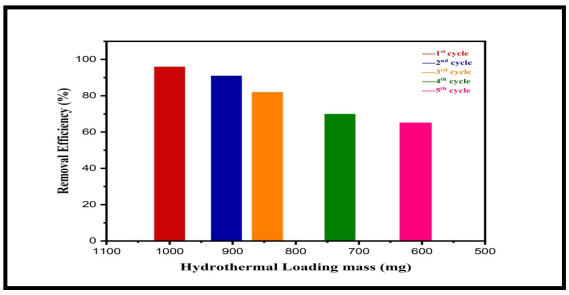


Fig 17: Hydrothermal regeneration of cashew nut shell activated carbon

Figure 17 shows the removal efficiency of CNS-AC over the five hydrothermal regeneration cycles, plotted against the hydrothermal loading mass (mg). The removal efficiency decreased gradually as the number of cycles increased.

Regeneration Efficiency and Adsorption Performance

In the first three cycles, CNS-AC retained high removal efficiencies of 96%, 91%, and 82%, respectively, indicating effective desorption of the adsorbed dye during hydrothermal treatment. The removal efficiency decreased further to 70% in the fourth cycle and 65% in the fifth cycle. Overall, the CNS-AC exhibited an average removal efficiency of approximately 81% over the five regeneration cycles**,** demonstrating its potential for repeated use. The gradual decline in removal efficiency may be attributed to the loss of a small amount of adsorbent during recovery and the possible blockage or alteration of active adsorption sites after repeated hydrothermal regeneration.

Effect of Hydrothermal Loading Mass

The x-axis suggests that adsorption performance varies slightly with loading mass (mg). Higher loading masses might lead to diffusion resistance and incomplete desorption during regeneration, reducing efficiency. This can be explained by:

The loading mass of CNS-AC decreased from 1000 mg in the first cycle to about 600 mg in the fifth cycle because of carbon loss during filtration and handling. Since the adsorbent dose decreases with each cycle, the number of available adsorption sites also decreases, which lowers the removal efficiency.

Diffusion Constraints:

Higher loading masses may lead to non-uniform exposure to hydrothermal conditions, causing incomplete contaminant desorption.

Competitive Adsorption:

As the available adsorption sites degrade, interactions between adsorbates become less favorable, further lowering efficiency.

Structural Stability and Reusability Potential

The observed efficiency trend suggests that CNS-AC can be effectively regenerated up to five cycles before significant degradation occurs.This aligns with BET surface area reduction and TGA analysis, where thermal stability is maintained for initial cycles but deteriorates with prolonged hydrothermal exposure.The results indicate that hydrothermal regeneration is a viable and sustainable method for CNS-AC reuse, though optimization of temperature, pressure, and treatment duration may extend regeneration limits.

CONCLUSION

Activated carbon derived from cashew nut shells (CNSAC) demonstrated high efficiency in the removal of Methylene Blue dye from aqueous solutions. Optimal adsorption conditions were identified at pH 12, with a maximum removal efficiency of 91%and adherence to the Langmuir isotherm model, indicating monolayer adsorption. Kinetic studies confirmed that the adsorption process follows a pseudo-second-order model, suggesting chemisorption as the rate-limiting step. CNSAC exhibited good stability and reusability, retaining 81% removal efficiency after fivehydrothermal regeneration cycles. Hydrothermal regeneration of CNS-AC retains substantial adsorption capacity for up to five regeneration cycles before structural and chemical degradation limits its reusability. The decline in efficiency is primarily attributed to pore collapse, functional group loss, and surface etching, which affect both physical and chemical adsorption mechanisms. The findings suggest that CNSAC is a viable, low-cost, and sustainable alternative for wastewater treatment applications, promoting environmental conservation and public health protection.

REFERENCES

1. Liu, Shanshan, HeyiGe, Cuicui Wang, Yu Zou, and Jingyu Liu. "Agricultural waste/graphene oxide 3D bio-adsorbent for highly efficient removal of methylene blue from water pollution." Science of the Total Environment 628 (2018): 959-968.
2. Kavil, Yasar N., Yasser A. Shaban, SaeedSaadAlelyani, Radwan Al-Farawati, Mohammad I. Orif, Mohammed A. Ghandourah, Mark Schmidt, Adnan J. Turki, and MousaZobidi. "The removal of methylene blue as a remedy of dye-based marine pollution: a photocatalytic perspective." Research on Chemical Intermediates 46 (2020): 755-768.
3. Rafatullah, Mohd, Othman Sulaiman, RokiahHashim, and Anees Ahmad. "Adsorption of methylene blue on low-cost adsorbents: a review." Journal of hazardous materials 177, no. 1-3 (2010): 70-80.
4. Chia, Chin Hua, NurFazlindaRazali, MohdShaifulSajab, SaraniZakaria, Nay Ming Huang, and Hong Ngee Lim. "Methylene blue adsorption on graphene oxide." SainsMalaysiana 42, no. 6 (2013): 819-826.
5. Ghosh, Dipa, and Krishna G. Bhattacharyya. "Adsorption of methylene blue on

kaolinite."Applied clay science 20, no. 6 (2002): 295-300.
6. Kheradmand, Asiyeh, MehrdadNegarestani, SimaKazemi, HadiShayesteh, ShahrzadJavanshir, and HosseinGhiasinejad. "Adsorption behavior of rhamnolipid modified magnetic Co/Al layered double hydroxide for the removal of cationic and anionic dyes." Scientific Reports 12, no. 1 (2022): 14623.
7. Kheradmand, Asiyeh, MehrdadNegarestani, AfsanehMollahosseini, HadiShayesteh, and HamidrezaFarimaniraad. "Low-cost treated lignocellulosic biomass waste supported with FeCl3/Zn (NO3) 2 for water decolorization." Scientific Reports 12, no. 1 (2022): 16442.
8. Al-Tohamy, Rania, Sameh S. Ali, Fanghua Li, Kamal M. Okasha, Yehia A-G. Mahmoud, Tamer Elsamahy, Haixin Jiao, Yinyi Fu, and Jianzhong Sun. "A critical review on the treatment of dye-containing wastewater: Ecotoxicological and health concerns of textile dyes and possible remediation approaches for environmental safety." Ecotoxicology and Environmental Safety 231 (2022): 113160.
9. Rathi, B. Senthil, P. Senthil Kumar, and Dai-Viet N. Vo. "Critical review on hazardous pollutants in water environment: Occurrence, monitoring, fate, removal technologies and risk assessment." Science of the Total Environment 797 (2021): 149134.
10. Shindhal, Toral, ParitaRakholiya, SunitaVarjani, Ashok Pandey, HuuHao Ngo, WenshanGuo, How Yong Ng, and Mohammad J. Taherzadeh. "A critical review on advances in the practices and perspectives for the treatment of dye industry wastewater."Bioengineered 12, no. 1 (2021): 70-87.
11. Periyasamy, Aravin Prince. "Recent advances in the remediation of textile-dye containing wastewater: prioritizing human health and sustainable wastewater treatment." Sustainability 16, no. 2 (2024): 495.
12. Piaskowski, Krzysztof, RenataŚwiderska-Dąbrowska, and Paweł K. Zarzycki. "Dye removal from water and wastewater using various physical, chemical, and biological processes." Journal of AOAC International 101, no. 5 (2018): 1371-1384.
13. Katheresan, Vanitha, JibrailKansedo, and Sie Yon Lau. "Efficiency of various recent wastewater dye removal methods: A review." Journal of environmental chemical engineering 6, no. 4 (2018): 4676-4697.
14. Yunusa, Umar, BishirUsman, and Muhammad Bashir Ibrahim. "Cationic dyes removal from wastewater by adsorptive method: A systematic in-depth review." Algerian Journal of Chemical Engineering AJCE 1, no. 2 (2021): 6-40.
15. Dutta, Soumi, Bramha Gupta, Suneel Kumar Srivastava, and Ashok Kumar Gupta. "Recent advances on the removal of dyes from wastewater using various adsorbents: A critical review." Materials Advances 2, no. 14 (2021): 4497-4531.
16. Monteil, Hélène, YoanPechaud, NihalOturan, and Mehmet A. Oturan. "A review on efficiency and cost effectiveness of electro- and bio-electro-Fenton processes: application to the treatment of pharmaceutical pollutants in water." Chemical engineering journal 376 (2019): 119577.
17. Chowdhury, ZairaZaman. Preparation, characterization and adsorption studies of heavy metals onto activated adsorbent materials derived from agricultural residues. University of Malaya (Malaysia), 2013.
18. Moosavi, Seyedehmaryam, Chin Wei Lai, SinyeeGan, GolnoushZamiri, OmidAkbarzadehPivehzhani, and MohdRafie Johan. "Application of efficient magnetic particles and activated carbon for dye removal from wastewater." ACS omega 5, no. 33 (2020): 20684-20697.
19. Arshanitsa, Alexandr, LilijaJashina, Matiss Pals, JevgenijaPonomarenko, YegorAkishin, and MajaZake. "Characteristics of the Main- and Side-Stream Products of Microwave Assisted Torrefaction of Lignocellulosic Biomass of Different Origination." Energies 15, no. 5 (2022): 1857.
20. Fakayode, OlugbengaAbiola, HafidaWahia, Lei Zhang, Cunshan Zhou, and Haile Ma. "State-of-the-art co-pyrolysis of lignocellulosic and macroalgae biomass feedstocks for improved bio-oil production-A review." Fuel 332 (2023): 126071.
21. Ceyhan, Ayhan Abdullah, ÖmerŞahin, OrhanBaytar, and CaferSaka. "Surface and porous characterization of activated carbon prepared from pyrolysis of biomass by two-stage procedure at low activation temperature and it's the adsorption of iodine." Journal of Analytical and Applied Pyrolysis 104 (2013): 378-383.
22. Cooper, Jason K., Alexandra M. Franco, SherazGul, CarleyCorrado, and Jin Z. Zhang. "Characterization of primary amine capped CdSe, ZnSe, and ZnS quantum dots by FT-IR: determination of surface bonding interaction and identification of selective desorption." Langmuir 27, no. 13 (2011): 8486-8493.
23. Podstawka, E., A. Kudelski, P. Kafarski, and L. M. Proniewicz. "Influence of aliphatic spacer group on adsorption mechanisms of phosphonate derivatives of l phenylalanine:

surface-enhanced Raman, Raman, and infrared studies." Surface science 601, no. 19 (2007): 4586-4597.
24. Esme, Asli. "Experimental (FT–IR, FT–Raman, and UV–Vis) and quantum chemical calculations on monomer and dimer structures of l-hydroxy-2-naphthoic acid using the DFT and TD–DFT methods." Indian Journal of Pure & Applied Physics (IJPAP) 57, no. 11 (2019): 822-835.
25. Hamza, Zahra M. "Study of Spectra Physical for Some Samples of Medical Herbal by FTIR-ATR Spectroscopy." Journal of Pharmaceutical Negative Results 13, no. 1 (2022): 49-55.
26. Yan, Wenchang, Dong Liu, Daoyong Tan, Peng Yuan, and Ming Chen. "FTIR spectroscopy study of the structure changes of palygorskite under heating." Spectrochimicaacta part A: molecular and biomolecular spectroscopy 97 (2012): 1052-1057.
27. Molavi, Hossein, AlirezaPourghaderi, and Akbar Shojaei. "Experimental study on the influence of initial pH, ionic strength, and temperature on the selective adsorption of dyes onto nanodiamonds." Journal of Chemical & Engineering Data 64, no. 4 (2019): 1508-1514.
28. Wang, Zihao, Mingming Wang, XiaomeiLyu, Caiyun Wang, Yanjun Tong, Xiao Hua, and Ruijin Yang. "Recycling preparation of high-purity tagatose from galactose using one-pot boronate affinity adsorbent-based adsorption-Assisted isomerization and simultaneous purification." Chemical Engineering Journal 446 (2022): 137089.
29. Moussout, Hamou, HammouAhlafi, Mustapha Aazza, and Hamid Maghat. "Critical of linear and nonlinear equations of pseudo-first order and pseudo-second order kinetic models." Karbala International Journal of Modern Science 4, no. 2 (2018): 244-254.
30. Robati, Dariush. "Pseudo-second-order kinetic equations for modeling adsorption systems for removal of lead ions using multi-walled carbon nanotube." Journal of nanostructure in Chemistry 3 (2013): 1-6.
31. Li, D., J. Yan, Z. Liu, and Z. Liu. "Adsorption kinetic studies for removal of methylene blue using activated carbon prepared from sugar beet pulp." International Journal of Environmental Science and Technology 13 (2016): 1815-1822.
32. Danish, Mohd, Khursheed B. Ansari, Mohammad Danish, AmnaKhatoon, Rifaqat Ali Khan Rao, SadafZaidi, and Rameez Ahmad Aftab. "A comprehensive investigation of external mass transfer and intraparticle diffusion for batch and continuous adsorption of heavy metals using pore volume and surface diffusion model." Separation and Purification Technology 292 (2022): 120996.
33. Kumar, PonnusamySenthil, SubramaniamRamalingam, and KannaiyanSathishkumar. "Removal of methylene blue dye from aqueous solution by activated carbon prepared from cashew nut shell as a new low-cost adsorbent." Korean Journal of chemical engineering 28 (2011): 149-155.
34. Ho, Yuh-Shan, and Gordon McKay. "Pseudo-second order model for sorption processes." Process biochemistry 34, no. 5 (1999): 451-465. 35. Kumar, A., Jena, H. M. (2016). Preparation and characterization of high surface area activated carbon from Fox nut (Euryale ferox) shell by chemical activation with H3PO4. Results in Physics, 6, 651-658.
36. Foo, K. Y., Hameed, B. H. (2012). Preparation, characterization and evaluation of adsorptive properties of orange peel based activated carbon via microwave induced K2CO3 activation. Bioresource Technology, 104, 679-686.
37. Prahas, D., Kartika, Y., Indraswati, N., &Ismadji, S. (2008). Activated carbon from jackfruit peel waste by H3PO4 chemical activation: Pore structure and surface chemistry characterization. Chemical Engineering Journal, 140(1-3), 32-42. 38. Ruthven, D. M. (1984). Principles of adsorption and adsorption processes. John Wiley & Sons.
39. Sing, K. S. (1985). Reporting physisorption data for gas/solid systems with special reference to the determination of surface area and porosity (Recommendations1984). Pure and Applied Chemistry,qtt